Letter to the Editor

Multimodality imaging of ureteral desmoplastic small round cell tumor: a case description and literature analysis of ^{18}F-fluoro-2-deoxy-d-glucose positron emission tomography-computed tomography findings

Wenpeng Huang[1], Yongbai Zhang[1], Yongkang Qiu[1], Yi Liu[2], Zhaonan Sun[3], Lele Song[1], Aixiang Wang[2], Jixin Zhang[4], Lei Kang[1]

[1]Department of Nuclear Medicine, Peking University First Hospital, Beijing, China; [2]Department of Urology, Peking University First Hospital, Beijing, China; [3]Department of Medical Imaging, Peking University First Hospital, Beijing, China; [4]Department of Pathology, Peking University First Hospital, Beijing, China

Correspondence to: Lei Kang, MD, PhD. Department of Nuclear Medicine, Peking University First Hospital, 8 Xishiku St., Xicheng District, Beijing 100034, China. Email: kanglei@bjmu.edu.cn; Jixin Zhang, MD. Department of Pathology, Peking University First Hospital, 8 Xishiku St., Xicheng District, Beijing 100034, China. Email: jixin.zhang@pkufh.cn; Aixiang Wang, MD. Department of Urology, Peking University First Hospital, 8 Xishiku St., Xicheng District, Beijing 100034, China. Email: wax20030826@126.com.

Submitted Nov 21, 2023. Accepted for publication Jan 26, 2024. Published online Mar 15, 2024.
doi: 10.21037/qims-23-1649
View this article at: https://dx.doi.org/10.21037/qims-23-1649

Introduction

The diagnosis of round cell sarcomas has undergone rapid evolution in the past decade, leading to significant diagnostic challenges for pathologists and oncologists. This transformation can be largely attributed to the introduction of next-generation sequencing techniques, enabling the identification of novel gene fusions in round cell sarcomas. Desmoplastic small round cell tumors (DSRCTs) constitute a rare subtype of soft tissue sarcoma, with an incidence ranging from 0.2 to 0.5 cases per million, and are associated with an aggressive clinical course (1). Gerald and Rosai initially described this disease in 1989 (2). DSRCT is characterized by an *EWSR1 Wilms tumor* 1 (*WT1*) translocation, resulting in a fusion protein that incorporates the *EWSR1* amino-terminus and the *WT1* carboxy-terminus, thereby confirming the diagnosis (3). DSRCT demonstrates a pronounced predilection for metastasis to various sites, particularly favoring the retroperitoneal lymph nodes and liver, with a notably higher incidence compared to lung involvement. The prevailing clinical manifestation of DSRCT is a multinodular growth involving the serosal surface, notably within the abdominal cavity. Indeed, involvement of the pleura, scrotum, ovary, liver, kidney, bone, and soft tissues of the hand, parotid gland, sinonasal tissues, intracranial tissues, and scalp soft tissues has also been documented (4). The diagnosis and staging of DSRCT have heavily relied on anatomic imaging. ^{18}F-fluoro-2-deoxy-d-glucose (^{18}F-FDG) positron emission tomography combined with computed tomography (PET/CT) has been proven to be valuable for assessing staging and the likelihood of tumor recurrence.

In this case report, we present an uncommon manifestation of ureteral DSRCT in a 63-year-old male, which underscores the diverse clinical and imaging features inherent in the manifestation of this disease. Importantly, in regard to DSRCT's rapid growth and tendency for widespread metastases, this case highlights the critical significance of early detection and prompt intervention.

Case presentation

All procedures performed in this study were in accordance with the ethical standards of the Medical Ethics Committee of Peking University First Hospital and with the Helsinki Declaration (as revised in 2013). Written informed consent

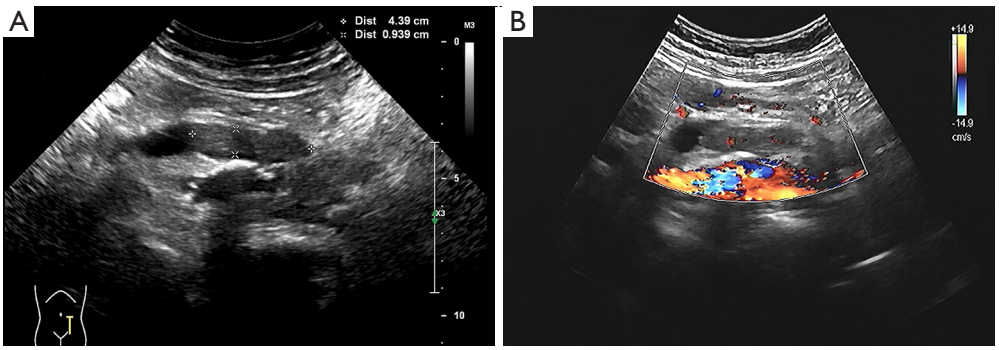

Figure 1 Ultrasound scanning of ureteral DSRCT (transverse view). (A) A hypoechoic mass measuring 3.92 cm × 1.47 cm in size was observed 5.0 cm from the left renal hilum-ureteral junction (within the ureter). (B) CDFI showed a class I flow signal within the lesion. DSRCT, desmoplastic small round cell tumor; CDFI, color Doppler flow imaging.

was obtained from the patient for publication of this case report and accompanying images. A copy of the written consent is available for review by the editorial office of this journal.

Clinical history

A 63-year-old male patient presented with a 5-month history of full-length hematuria visible to the naked eye without any obvious trigger, accompanied by urinary frequency but without symptoms of painful urination. The patient had a history of diffuse large B-cell lymphoma (DLBCL), which was successfully treated 15 years prior with autologous hematopoietic stem cell transplantation following eight cycles of the rituximab, cyclophosphamide, doxorubicin, vincristine, and prednisone (R-CHOP) regimen. The patient had an Eastern Cooperative Oncology Group (ECOG) performance status of 1. Examination revealed no tenderness to percussion in the bilateral renal regions, no pressure in the bilateral ureteral tracts, and no suprapubic bladder bulging. Urine exfoliative cytology yielded negative results.

Imaging studies

A urologic ultrasound examination revealed dilation in the upper left ureter, characterized by an internal diameter of approximately 1.60 cm. Additionally, a hypoechoic mass measuring 3.92 cm × 1.47 cm was observed 5.0 cm from the left renal hilum-ureteral junction (within the ureter), displaying a class I blood flow signal on color Doppler flow imaging (CDFI). Adjacent to the left renal hilum, an enlarged hypoechoic lymph node measuring about 2.33 cm in diameter was identified (*Figure 1*). Computed tomography urography (CTU) revealed a soft tissue density mass within the lumen of the left mid-ureter, appearing as a strip measuring approximately 1.20 cm at its widest point, with a measured area of involvement of about 4.10 cm. The CT attenuation values were 42 Hounsfield units (HU) in the plain phase, 73 HU in the corticomedullary phase, and 70 HU in the nephrographic phase, with enhancement scans displaying moderate enhancement. Both the ureter and the renal calyces above the lesion exhibited dilation and hydronephrosis, contributing to a reduction in both volume and perfusion of the left kidney. Adjacent to the abdominal aorta and left iliac vessels, multiple enlarged lymph nodes were evident (*Figure 2*).

To further clarify the staging, the patient underwent ^{18}F-FDG PET/CT for assessment of the lesions. PET images depicted lesions confined to the ureteral lumen with increased ^{18}F-FDG uptake, registering a maximum standardized uptake (SUVmax) value of 10.5 and a total lesion glycolysis (TLG) value of 28.5 during the conventional imaging phase (60 minutes postinjection). The delayed imaging phase (210 minutes postinjection) yielded an SUVmax value of 20.1 and a TLG value of 41.4. Additionally, multiple enlarged and fused lymph nodes were noted along the abdominal aorta and inferior vena cava and adjacent to the left iliac vessels, which exhibited a heterogeneous increase in ^{18}F-FDG uptake. SUVmax values ranged from 9.1 to 10.6 in the routine imaging phase and increased to a range of 13.4 to 19.1 in the delayed imaging phase (*Figure 3*). The imaging diagnosis confirmed a malignant tumor of the left ureter accompanied by multiple

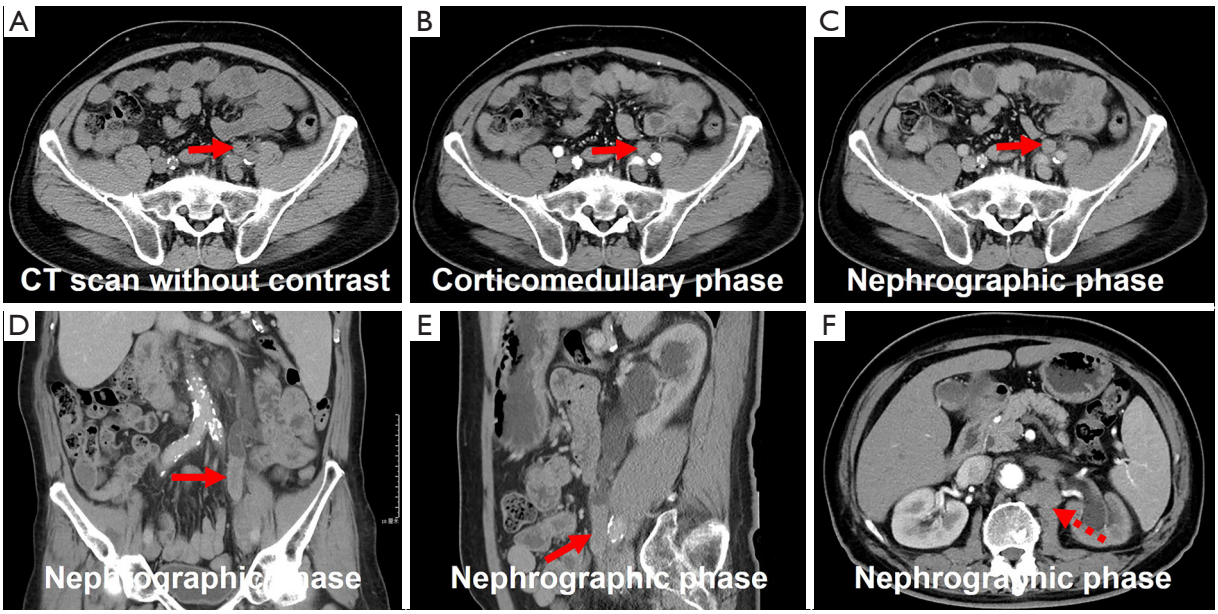

Figure 2 Computed tomography urography imaging of ureteral DSRCT. (A-C) Transverse images revealed a soft tissue density mass restricted to the lumen of the left mid-ureter (long arrows), with a CT attenuation value of 42 HU in the plain phase and 73 and 70 HU in the corticomedullary and nephrographic phases, respectively. (D,E) Coronal and sagittal images from the nephrographic phase revealed the lesion (long arrows) to be striated and measuring approximately 1.20 cm at its widest point, with an area of involvement estimated at around 4.10 cm; enhancement scans displayed moderate enhancement. (F) Transverse images revealed the presence of enlarged lymph nodes adjacent to the abdominal aorta (dashed arrow). CT, computed tomography; DSRCT, desmoplastic small round cell tumor; HU, Hounsfield unit.

lymph node metastases.

Pathology

The patient underwent a CT-guided puncture biopsy of the left inguinal lymph node. Microscopically, the lymph node structure remained intact, displaying scattered lymphoid follicles, atrophied germinal centers, and fibrotic tissue hyperplasia in the interfollicular zone accompanied by plasma cell infiltration. Notably, no tumor cells were observed (*Figure 4A*,*4B*). Immunohistochemistry revealed positive expression of CD3, CD20, CD21 [highlighting the follicular dendritic cell (FDC) network], CD138, immunoglobin G (IgG), and key performance indicators (KPIs) (highlighting the histiocytes) (*Figure 4C-4H*). Additionally, 10% of the tumor cells demonstrated positivity for Ki-67 (*Figure 4I*). The possibility of DLBLC recurrence was excluded. The patient underwent further ureteroscopy with biopsy for pathology. Microscopic examination revealed infiltrative growth of poorly differentiated neoplastic cells forming nests, cords, and sheets within a desmoplastic stroma. (*Figure 5A*,*5B*). Immunohistochemistry showed positive expression of desmin, vimentin, synuclein (SYN), and cytokeratin (CK)8/18 (*Figure 5C-5G*). Fluorescence in situ hybridization (FISH) analysis with a break-apart probe confirmed the presence of *EWSR1* and *WT1* gene rearrangements in the neoplastic cells. The conclusive diagnosis was DSRCT of the ureter.

Treatment and follow-up

After completing six cycles of chemotherapy consisting of bevacizumab (400 mg) on day 1 + paclitaxel (300 mg) on day 1 + gemcitabine (1.6 g) on days 1 and 8, the patient underwent a follow-up CTU. The results revealed a significant reduction in the size of the ureteral lesion and metastatic lymph nodes compared to the previous scan (*Figure 6*), with the treatment efficacy evaluated as partial remission (PR). Subsequently, the patient received whole abdominopelvic intensity-modulated radiotherapy (62.5 Gy/25 fractions/5 weeks). One month later, urologic magnetic resonance urography (MRU) demonstrated a marked reduction in the size of the lesion (*Figure 7*). As of this writing, the patient is currently alive and well and continues to be under regular follow-up.

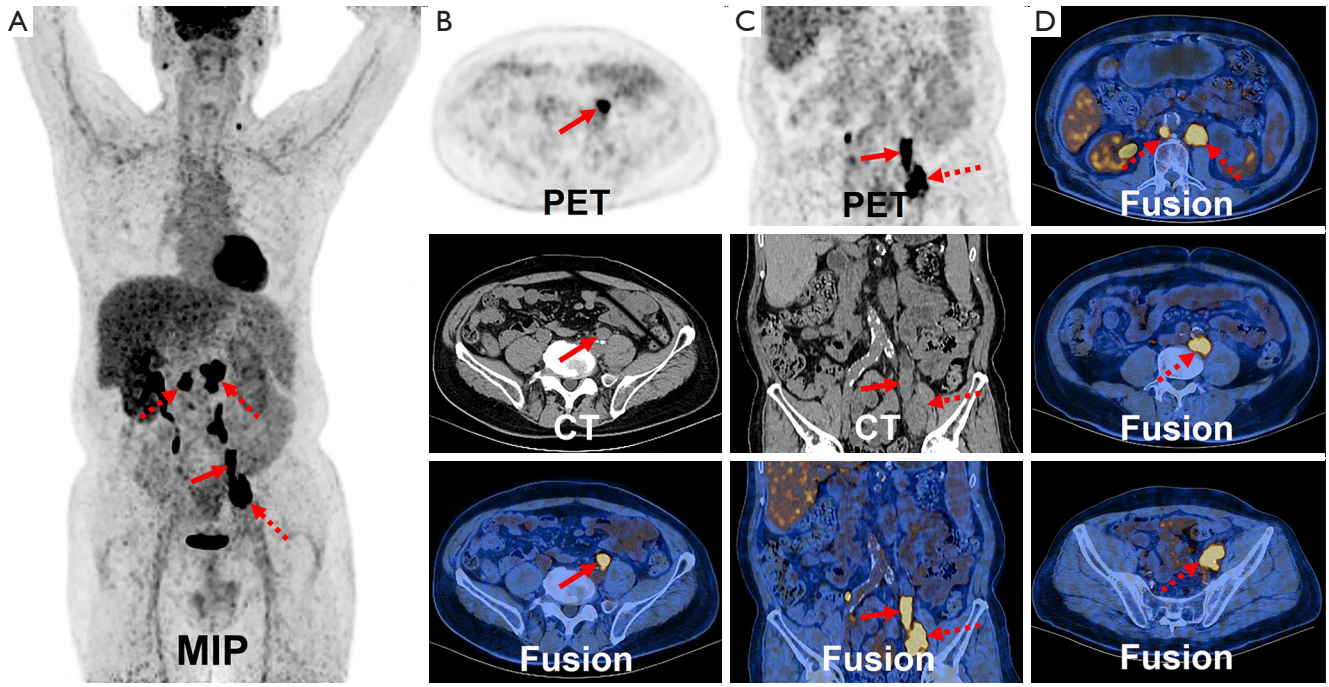

Figure 3 ^{18}F-FDG PET/CT imaging of ureteral DSRCT. (A) The anteroposterior 3-dimensional MIP demonstrated increased metabolic activity in the middle ureter (long arrow), paraaortic lymph nodes, and left iliac vascular lymph nodes (dashed arrows). (B,C) Transverse images and coronal images showed lesions (long arrows) confined to the ureteral lumen with increased ^{18}F-FDG uptake, with SUVmax values of 10.5, and a heterogeneous increase in ^{18}F-FDG uptake in the left inguinal lymph node (dashed arrows), with SUVmax values of 11.3. (D) Transverse images showed a heterogeneous increase in ^{18}F-FDG uptake in the lymph nodes adjacent to the abdominal aorta (dashed arrows), with SUVmax values of 10.6. MIP, maximum intensity projection image; PET/CT, positron emission tomography-computed tomography; ^{18}F-FDG, ^{18}F-fluoro-2-deoxy-d-glucose; DSRCT, desmoplastic small round cell tumor; SUVmax, maximum standardized uptake value.

Discussion

Those with DLBCL face an elevated risk of developing secondary primary malignancies (SPMs) throughout their lifetimes, including cancers affecting the stomach, colorectum, and lungs. The etiology of SPMs after DLBCL is multifactorial, attributed to a combination of factors such as exposure to chemotherapy, radiation, and rituximab and associated immunosuppression; chronic infections; lifestyle practices; demographics; and genetic susceptibility (5). The findings by Major *et al.* indicate that with prolonged survival in patients with DLBCL, the risk of SPM development varies according to their stage at diagnosis and the time elapsed since diagnosis (6). Our patient had been successfully treated for DLBCL 15 years prior to his attending our center. This emphasizes the importance of raising awareness about the heightened risk of subsequent malignancies for DLBCL survivors and their physicians.

DSRCT, as per the International Classification of Disease for Oncology (2020), is classified as a malignant tumor of uncertain differentiation (7). It predominantly occurs in adolescent and young adult males. Compared to that in the adolescent or young adult population, DSRCT in those of older age is associated with both an unusual location and presentation and is more common. The tumor exhibits highly aggressive behavior, with widespread peritoneal seeding at presentation. The exact tissue of origin remains unknown. Upon diagnosis, over 90% of patients with DSRCT have synchronous peritoneal metastases, with approximately 50% having synchronous extraperitoneal metastases, often affecting the liver, lungs, bone, and bone marrow. Consequently, the disease is frequently categorized as stage IV at the time of diagnosis. DSRCT typically manifests as abdominal pain, distension, and masses causing secondary pressure symptoms. Physical examination may reveal a palpable mass in the abdominal or pelvic cavity, and involvement of the bladder, ureters, prostate, and paratesticular structures is not uncommon.

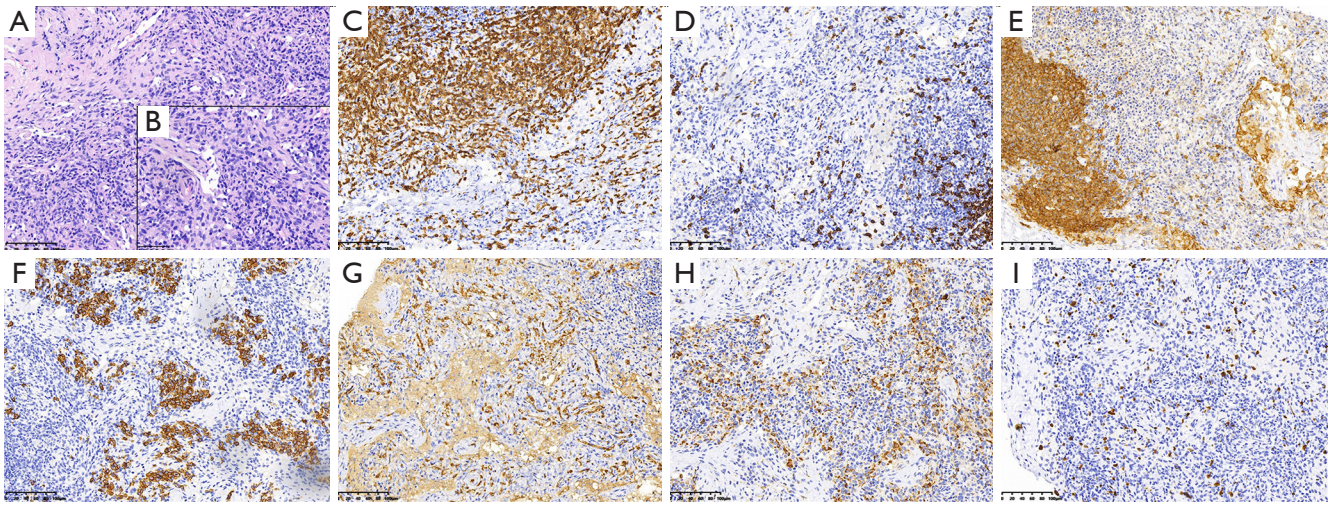

Figure 4 Histopathological and immunohistochemical images of the CT-guided puncture biopsy of the left inguinal lymph node. (A,B) HE staining (magnification 200× and 400×) indicated an intact lymph node structure, with scattered lymphoid follicles, atrophied germinal centers, and fibrotic tissue hyperplasia in the interfollicular zone, accompanied by plasma cell infiltration. Notably, no tumor cells were observed. (C-H) Immunohistochemistry showed that the tumor cells were positive for CD3, CD20, CD21 (highlighting the FDC network), CD138, IgG, and KPI (highlighting the histiocytes) (Envision, magnification 200×). (I) Ki-67 was observed to be positive in 10% of the tumor cells (Envision, magnification 200×). CT, computed tomography; HE, hematoxylin and eosin; FDC, follicular dendritic cell; IgG, immunoglobin G; KPI, key performance indicator.

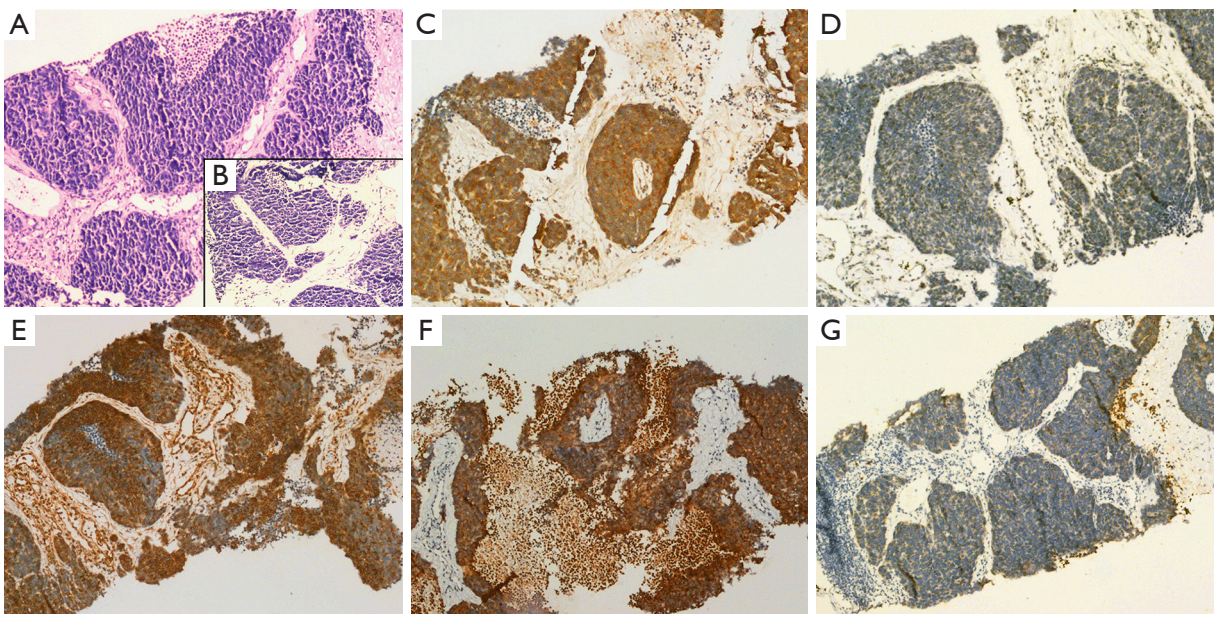

Figure 5 Histopathological and immunohistochemical images of ureteral DSRCT. (A,B) HE staining (magnification 100× and 200×) showed infiltrative growth of poorly differentiated neoplastic cells forming nests, cords, and sheets within a desmoplastic stroma. (C-G) Immunohistochemistry showed that the tumor cells were positive for desmin, vimentin, SYN, and CK8/18 (magnification 100×). DSRCT, desmoplastic small round cell tumor; HE, hematoxylin and eosin; SYN, synuclein; CK8/18, cytokeratin 8/18.

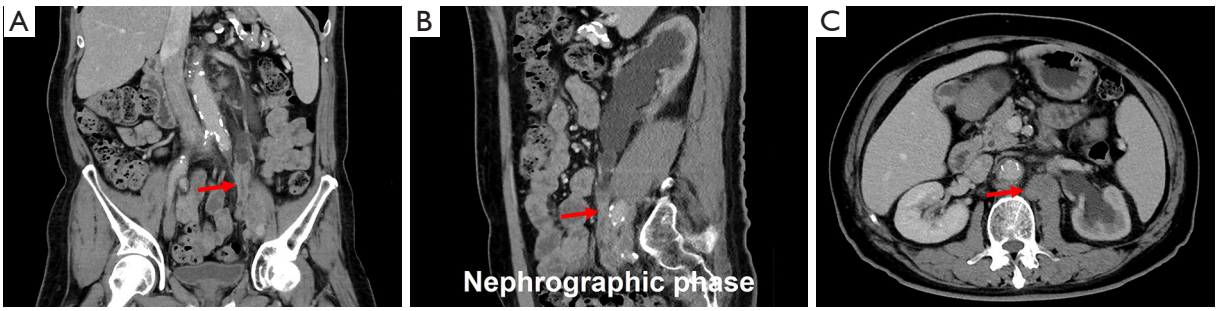

Figure 6 Computed tomography urography imaging of ureteral DSRCT after chemotherapy. (A,B) Coronal and sagittal images from the nephrographic phase revealed a significant reduction in the size of the ureteral lesion (long arrows). (C) The size of the lymph nodes (long arrow) adjacent to the abdominal aorta had significantly diminished compared to the previous assessment, and necrosis and cystic changes were apparent in the lymph nodes. DSRCT, desmoplastic small round cell tumor.

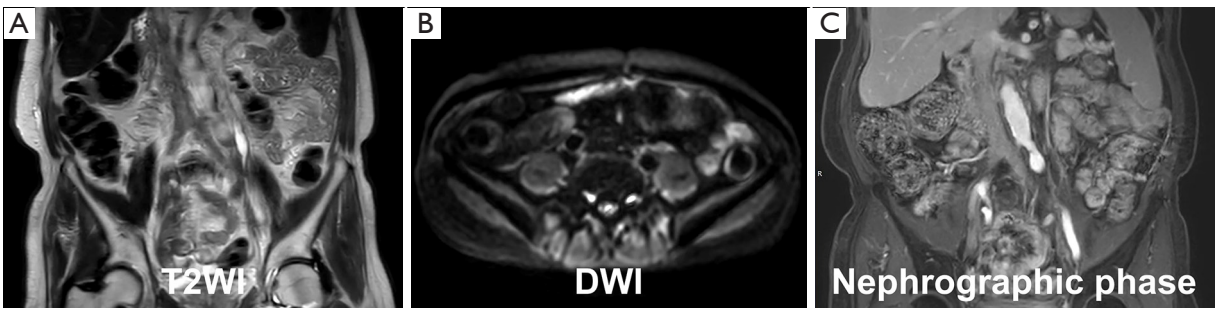

Figure 7 Magnetic resonance urography imaging of ureteral DSRCT after chemotherapy and intensity-modulated radiotherapy. (A-C) T2WI, DWI, and fat-sat Gd-T1WI images showed a marked reduction in the size of the ureteral lesion. T2WI, T2-weighted imaging; DWI, diffusion-weighted imaging; DSRCT, desmoplastic small round cell tumor; fat-sat Gd-T1WI, fat-saturated gadolinium-enhanced T1-weighted imaging.

However, primary DSRCT in the ureter is rare. Our case had hematuria and metastases to the paraaortic and inguinal lymph nodes, which are typical sites within the ureteral lymph node drainage zones. Consideration of the typical lymph node drainage pattern is essential for managing both left and right ureteral tumors.

DSRCT belongs to the family of small round blue cell tumors and exhibits unique clinical, histologic, immunohistochemical, cytogenetic, and molecular features (1,3). Histologically, nests of small round tumor cells that coexpress epithelial, mesenchymal, and neural cell markers are surrounded by a cellular desmoplastic stroma, demonstrating commonalities with other round cell tumors. The gold standard for diagnosing DSRCT is the combination of histopathology and cytogenetics. It is crucial to acknowledge that DSRCT exhibits a polyphenotypic immune profile and considerable morphologic variation both among tumors and within the same neoplasm. The immunophenotype of DSRCT is marked by a polyphenotypic immune profile, encompassing epithelial markers [CK and epithelial membrane antigen (EMA)], neural markers [CD56 and neuron-specific enolase (NSE)], and muscle markers (vimentin and desmin), along with notable morphological diversity among tumors and within the same neoplasm (8). Smaller subsets express chromogranin, synaptophysin, CD56, neurofilament protein, and S100 protein. DSRCT is differentiated from other small round blue cell tumors by the presence of the *t(11;22)(p13:q12)* chromosomal translocation (9).

Symptoms that are associated with the tumor burden and location of DSRCT warrant prompt investigation through imaging examinations. Current imaging techniques for assessing ureteral tumors include ultrasound, CT, and magnetic resonance imaging (MRI). The diagnosis and staging of DSRCT heavily rely on anatomic imaging. The most prevalent imaging finding is the existence of

multiple, lobulated, low-attenuation, and heterogeneous peritoneal, omental, or serosal soft tissue masses (10). The manifestation of DSRCT as a solitary peritoneal mass is considered rare. Pickhardt *et al.* (11) reported that two out of nine patients in their DSRCT series presented with a solitary peritoneal mass. In contrast, we have not observed such cases; rather, our patient had a limited mass in the ureter.

Tumors often manifest with inhomogeneous attenuation on CT, with areas of central low attenuation corresponding to focal hemorrhage within the tumor on gross pathologic analysis. CT findings are considered nonspecific and also applicable to other conditions, such as peritoneal carcinomatosis. The MRI characteristics of DSRCT encompass intermediate signal intensity on T1-weighted images and high signal intensity on T2-weighted images. The observed enhancement pattern on MRI may be attributable to tumor heterogeneity, as exemplified by our patient, with inhomogeneous mild enhancement being present on gadolinium-enhanced T1-weighted images, which was associated with the supply to the ureteral tumor by the thin blood vessels.

CT and MRI serve as valuable tools for identifying disease sites, but their capability to depict the viability and metabolic activity of tumors is limited. This limitation underscores the significance of employing ^{18}F-FDG PET/CT in DSRCT. FDG PET/CT holds a crucial role in the initial disease identification, assessment of tumor extent, and overall management of DSRCT. The integrated ^{18}F-FDG PET/CT stands out as the foremost functional and metabolic imaging technique, providing clinicians with comprehensive and precise information (12). Additionally, it can identify early tumor recurrence or progression ahead of morphologic changes visible on anatomic imaging. FDG PET/CT also functions as a predictor of extended disease-free survival or remission in patients who demonstrate a complete metabolic response (13,14). On FDG PET/CT scans, DSRCT typically displays increased FDG uptake, with variable SUVmax values of the masses, often reaching up to 24.66, indicative of a robust hypermetabolic trend (15). In the interpretation of PET/CT images, a differential diagnosis of DSRCT should be considered if increased FDG uptake in the ureter is encountered. A growing number of studies strongly support the use of PET/CT for staging (13-37), and we present a summary of the English literature on the clinical utility of this technique in patients with DSRCT in *Table 1* (38-46).

The prognosis for patients diagnosed with DSRCT is currently exceedingly grim, with only 29% surviving up to 3 years, and the 5-year overall survival rate falling within the range of 10–20% (47). In many medical centers, an Ewing sarcoma-based regimen is frequently employed as the initial treatment approach. Typically, the disease is addressed with an aggressive multimodal strategy that includes high-dose multiagent chemotherapy (vincristine, doxorubicin, cyclophosphamide, ifosfamide/mesna, and etoposide), surgery, and conformal external beam radiation. In patients with unresectable or metastatic disease, symptom control takes precedence, as treatment modalities have minimal impact on survival. Palliative chemotherapy (primarily monotherapy) is preferable.

In our case, treatment with the bevacizumab + paclitaxel + gemcitabine chemotherapy regimen resulted in a good remission, which was followed by an apparent macroscopical complete remission after the administration of local radiation therapy. In our decision-making process, we carefully considered the patient's renal function, recognizing the potential impact of long-term hydronephrosis on kidney health. In selecting the chemotherapy regimen, we also took into account the patient's renal function. Ifosfamide, a commonly used chemotherapy agent, can indeed pose challenges in patients with compromised renal function. Any novel medical treatment strategy for DSRCT must be seamlessly integrated with measures of local control, which remain a cornerstone in the management of this tumor type. In cases of unresectable or metastatic disease, prioritizing symptom control becomes paramount, as treatment modalities minimally impact overall survival. Palliative chemotherapy, primarily in the form of monotherapy, is deemed preferable. Indeed, the implementation of intensive induction medical therapies, followed by extensive local interventions, has demonstrated the potential to achieve apparent macroscopical complete remission in numerous DSRCT cases. However, in many instances, the primary obstacle to cure appears to be minimal residual disease, which resistant to initial therapeutic interventions (48). In such scenarios, the utilization of the bevacizumab + paclitaxel + gemcitabine chemotherapy regimen has shown promise, resulting in a substantial remission. In our case, this positive response was further consolidated by the administration of local radiation therapy, leading to an apparent macroscopical complete remission. With regard to targeted or nonconventional chemotherapy, there are other established agents, such as trabectedin and pazopanib, which have been approved for certain cases. Prexasertib (PRX) is a checkpoint kinase 1 (CHK1) inhibitor, and translocation-

Table 1 ^{18}F-FDG PET/CT manifestations of desmoplastic small round cell tumors

Case	Authors	Gender	Age	Clinical symptoms	Primary sites	Invasion and metastasis	Maximum diameter/cm	SUVmax	Management	Outcome
1	Zhang *et al.* (16)	M	26 y	NA	Abdomen-pelvis	NA	NA	12.7	NA	NA
2	Ostermeier *et al.* (14)	M	11 y	NA	Abdomen-pelvis	Liver	NA	10.0	Surgery	Alive at 7.5 y
3	Ostermeier *et al.* (14)	M	11 y	NA	Abdomen	Thorax	NA	10.7	Chemotherapy + radiotherapy	Died at 1.3 y
4	Ostermeier *et al.* (14)	M	20 y	NA	Supraclavicular mass	NA	NA	11.7	Surgery	Alive at 6 y
5	Ostermeier *et al.* (14)	M	20 y	NA	Abdomen	NA	NA	19.1	Surgery	Alive at 4 y
6	Ostermeier *et al.* (14)	M	2 y	NA	Right orbit	NA	NA	6.4	Surgery	Alive at 3 y
7	Ostermeier *et al.* (14)	M	16 y	NA	Abdomen-pelvis	NA	NA	8.4	NA	NA
8	Ostermeier *et al.* (14)	F	20 y	NA	Abdomen-pelvis	Thorax	NA	15.6	NA	Alive at 2 y
9	Kis *et al.* (17)	M	29 y	Right upper quadrant discomfort	Pelvis	Retroperitoneal lymph nodes	NA	16.5	Chemotherapy	NA
10	Xuesong *et al.* (18)	M	33 y	Left lower limb pain	Left upper tibial	NA	6.9	24.66	Surgery + chemotherapy	Alive at 18 mo
11	Kushner *et al.* (19)	M	18 y	NA	Abdomen-pelvis	Liver	NA	10.5	Surgery + chemotherapy + radiotherapy	Alive at 5.5 y
12	Reisner *et al.* (20)	M	27 y	Abdominal pain	Abdomen	Left paraaortic lymph nodes	11.1	10.2	Surgery + chemotherapy	Alive at 8 mo
13	Ben-Sellem *et al.* (13)	M	43 y	NA	Abdomen	Retroperitoneal lymph nodes	7	NA	Surgery + chemotherapy	Alive at 10 y.
14	Hatanaka *et al.* (21)	M	49 y	A mass in the right parotid gland without pain	Right parotid gland	NA	NA	NA	Surgery + radiotherapy	Alive at 3 y
15	de Araújo *et al.* (22)	M	37 y	Poor digestion and weight loss	Abdomen	Liver and peritoneum	7.0	Poor FDG avidity	Chemotherapy	Died at 34 mo
16	Chen *et al.* (23)	M	9 y	Abdomen mass	Kidney	Left supraclavicular and upper mediastinal lymph nodes	16.1	10.2	Surgery + chemotherapy	Alive at 1 y
17	Liu *et al.* (15)	F	30 y	Cough, sputum, and dyspnea	Kidney	Lung, spines, ribs and cervical lymph nodes	10.7	20.9	Surgery	NA
18	Harindran *et al.* (24)	M	42 y	Abdominal pain	Abdomen	Liver, spleen, mesentery, and bone marrow	NA	NA	Chemotherapy	NA
19	Harindran *et al.* (24)	M	21 y	Increased frequency of stools	Pelvis	Lung, mesentery, and bone marrow	NA	NA	Chemotherapy	NA

Table 1 (*continued*)

Table 1 (*continued*)

Case	Authors	Gender	Age	Clinical symptoms	Primary sites	Invasion and metastasis	Maximum diameter/cm	SUVmax	Management	Outcome
20	Harindran *et al.* (24)	M	20 y	Low backache and altered bowel habits	Rectum	Peritoneum, liver, and bone marrow	NA	NA	Chemotherapy	NA
21	Mathys *et al.* (25)	M	43 y	Paresthesia, numbness, pain and atrophy in right hand and arm	Right brachial plexus	NA	NA	NA	Surgery + radiotherapy	Alive at 18 mo
22	Fan *et al.* (26)	M	26 y	Colicky lower abdominal pain, right iliac fossa pain, anorexia, and nausea	Colon	NA	NA	NA	Surgery + chemotherapy	Alive at 6 mo
23	Fan *et al.* (26)	M	14 y	NA	Pelvis	Right common iliac vein lymph nodes	NA	NA	Surgery + chemotherapy	Alive at 20 mo
24	Fan *et al.* (26)	M	21 y	Left inguinal lymphadenopathy associated with pain	NA	Pelvis, left external iliac and paraaortic lymph nodes	NA	NA	Surgery + chemotherapy	Alive at 25 mo
25	Brunetti *et al.* (27)	M	20 y	NA	Abdomen	NA	12	11.6	Surgery + chemotherapy + target therapy	Alive at 6 mo
26	Asadbeigi *et al.* (28)	M	15 y	Left shoulder and lower back pain	Left shoulder	NA	1.5	NA	Surgery + chemotherapy	Alive at 2 y
27	Makis *et al.* (29)	M	41 y	NA	Abdomen	Pelvis and bones	25	18.5	Surgery + chemotherapy + radiotherapy	Died at 20 mo
28	Küpeli *et al.* (30)	M	16 y	A tough swelling on the left side of his face	Left face	Left inguinal lymph nodes and plantar face of the left foot	NA	NA	Surgery + chemotherapy	Died at 22 mo
29	Ramspott *et al.* (31)	M	69 y	Abdominal pain	Peritoneum	Pancreas	5	NA	Surgery + chemotherapy	Died at several weeks
30	Hassan *et al.* (32)	M	NA	Nausea, vomiting, and constipation	Colon	Liver, peritoneum, and lung	NA	9.9	Chemotherapy + target therapy	Died
31	Cracco *et al.* (33)	M	51 y	Reflux and intermitted mild abdominal pain	Colon	Liver	NA	NA	Surgery + chemotherapy	Alive at 24 mo
32	Zhou *et al.* (34)	M	26 y	Right submandibular mass	Right submandibular region	NA	2.8	NA	Surgery + chemotherapy + radiotherapy	Alive

Table 1 (*continued*)

Table 1 (*continued*)

Case	Authors	Gender	Age	Clinical symptoms	Primary sites	Invasion and metastasis	Maximum diameter/cm	SUVmax	Management	Outcome
33	Vujić *et al.* (35)	F	19 y	Abdominal distension	Abdomen	Ovaries and paraaortic lymph nodes	NA	NA	Surgery + chemotherapy	Alive at 12 mo
34	Subbiah *et al.* (36)	M	16 y	Abdominal distension and dyspnea	Abdomen	NA	28	NA	Chemotherapy + target therapy + surgery + radiotherapy	Alive
35	Umeda *et al.* (37)	M	16 y	Abdominal pain, weight loss, dyschezia, and hematochezia	Pelvis	Liver, bone, brain, and lymph nodes	NA	NA	Surgery + chemotherapy + target therapy	Died at 21 mo
36	Miwa *et al.* (38)	M	29 y	Pain, numbness and atrophy in left arm	Left brachial plexus	NA	NA	NA	Chemotherapy	Alive at 46 mo
37	Bengu Cobanoglu *et al.* (39)	M	4 y	Ptosis of the right eye	Right eye	NA	3.2	NA	Proton therapy + chemotherapy + surgery	Alive at 1 y
38	Piciu *et al.* (40)	F	58 y	Diffuse abdominal and bone pain, weight loss, and an enlargement of the abdomen, asthenia, cough and nausea	Retroperitoneal	Bones and lymph nodes	NA	NA	NA	NA
39	Laurens *et al.* (41)	F	56 y	NA	Abdomen	NA	NA	NA	Surgery	NA
40	Gan *et al.* (42)	M	29 y	A left neck mass	Pancreas	Abdomen and retroperitoneal and cervical lymph nodes	NA	NA	Chemotherapy	Alive at 9 mo
41	Çolak *et al.* (43)	F	40 y	NA	Right thigh	NA	6	Poor FDG avidity	Surgery	Alive
42	Hou *et al.* (44)	F	33 y	Cough and hemoptysis	Lung	Bones and left supraclavicular soft tissue	4.2	10.6	NA	NA
43	Sharma *et al.* (45)	M	18 y	Left knee and thigh pain	Left femur	Appendicular bones, calvarial soft tissue, mediastinum, lung, myocardium, and supraclavicular/pulmonary hilar nodes	NA	4.95	Chemotherapy + radiotherapy	Alive at 5 mo
44	Zheng *et al.* (46)	F	24 y	Lower abdominal pain	Ovary	NA	9.5	17.8	Surgery + chemotherapy	Alive at 10 mo

^{18}F-FDG, ^{18}F-fluoro-2-deoxy-d-glucose; PET/CT, positron emission tomography-computed tomography; SUVmax, maximum standardized uptake value; M, male; F, female; NA, not applicable; y, year; mo, month.

driven sarcomas exhibit elevated levels of replication stress, demonstrating susceptibility to CHK1 inhibition in preclinical models. A promising phase I/II study targeting CHK1 with PRX conducted at Memorial Sloan Kettering Cancer Center (MSKCC) has yielded results exceeding expectations (49). Unlike Ewing sarcoma, PRX seems to yield 4–5 months of progression-free survival in the second or third-line setting.

It is important to acknowledge that tumor recurrence is commonplace, with the majority of patients experiencing recurrence within months of complete cytoreductive surgery. In our case, the multidisciplinary team, in collaboration with the patient, chose a neoadjuvant chemotherapy approach before contemplating surgical intervention. This decision was grounded in the objective of reducing tumor size, aiming to facilitate a more manageable and successful surgical resection. However, for patients with extraperitoneal metastasis, surgery does not confer any benefits. It is worth noting that in a phase I trial, SU101, an inhibitor of the platelet-derived growth factor (PDGF) receptor pathway, yielded rapid symptom improvement and prolonged disease stabilization in a patient with refractory progressive DSRCT (50). The second-line regimens used for Ewing sarcoma have also shown benefit in DSRCT. Subbiah *et al.* (47) identified that in patients with extensive hepatic DSRCT metastases, survival can be prolonged by halting the progression of metastatic cancer to the liver through the use of ^{90}Y-microsphere radioembolization therapy. A phase I trial of intraperitoneal radioimmunotherapy with ^{131}I-8H9 is underway in patients with DSRCT, demonstrating good tolerability. Fine *et al.* (51) identified androgen receptors in 10 out of 27 patients with DSRCT, and *in vitro* assays demonstrated the growth of tumor cells when stimulated with dihydrotestosterone, indicating their functionality. Among the six patients with confirmed androgen receptor expression, three received androgen blockade and maintained stable disease for 3–6 months after progression on conventional treatment. We recommend referring patients with DSRCT to a tertiary cancer center experienced in treating this rare sarcoma. For instance, in the United States, the MSKCC and MD Anderson Cancer Center each manage approximately 20 DSRCT cases annually and stand among the select centers offering dedicated clinical trials for DSRCT. To date, limited biological data are available regarding the somatic genetics and epigenetics of DSRCT. Extensive international cooperation has the potential to enhance our understanding of the pathogenesis of DSRCT, explore new molecular targets, and identify potentially effective biological agents for this aggressive disease.

Conclusions

Primary DSRCT of the ureter is exceptionally rare and poses challenges for core biopsy specimens. DSRCT is a remarkable mimicker, easily confounded with more prevalent ureteral diseases such as ureteral epithelial cancer, polyps, amyloidosis, inflammation, and endometriosis. Long-term follow-up is imperative to monitor the likelihood of recurrence and metastasis. In this report, we present a patient who, as of this writing, shows no evidence of tumor recurrence, emphasizing the necessity for radiologists to be cognizant of the potential for a varied clinical course and imaging presentation associated with DSRCT. Clinical vigilance, identification, and multimodal therapy are essential to improving patient prognosis. Additional multi-institutional studies investigating the prognostic potential of FDG PET/CT findings could prove valuable for informing future approaches to disease management.

Acknowledgments

Funding: This work was supported by the National Natural Science Foundation of China (No. 82171970), the Beijing Science Foundation for Distinguished Young Scholars (No. JQ21025), and Interdisciplinary Research Project of Peking University First Hospital (No. 2023IR17).

Footnote

Conflicts of Interest: All authors have completed the ICMJE uniform disclosure form (available at https://qims.amegroups.com/article/view/10.21037/qims-23-1649/coif). The authors have no conflicts of interest to declare.

Ethical Statement: The authors are accountable for all aspects of the work in ensuring that questions related to the accuracy or integrity of any part of the work are appropriately investigated and resolved. All procedures performed in this study were in accordance with the ethical standards of the Medical Ethics Committee of Peking University First Hospital and with the Helsinki Declaration (as revised in 2013). Written informed consent was obtained from the patient for publication of this case report and accompanying images. A copy of the written consent is

available for review by the editorial office of this journal.

References

1. da Silva RC, Medeiros Filho P, Chioato L, Silva TR, Ribeiro SM, Bacchi CE. Desmoplastic small round cell tumor of the kidney mimicking Wilms tumor: a case report and review of the literature. Appl Immunohistochem Mol Morphol 2009;17:557-62.
2. Gerald WL, Rosai J. Case 2. Desmoplastic small cell tumor with divergent differentiation. Pediatr Pathol 1989;9:177-83.
3. Wang LL, Perlman EJ, Vujanic GM, Zuppan C, Brundler MA, Cheung CR, Calicchio ML, Dubois S, Cendron M, Murata-Collins JL, Wenger GD, Strzelecki D, Barr FG, Collins T, Perez-Atayde AR, Kozakewich H. Desmoplastic small round cell tumor of the kidney in childhood. Am J Surg Pathol 2007;31:576-84.
4. Ertoy Baydar D, Armutlu A, Aydin O, Dagdemir A, Yakupoglu YK. Desmoplastic small round cell tumor of the kidney: a case report. Diagn Pathol 2020;15:95.
5. Tao L, Clarke CA, Rosenberg AS, Advani RH, Jonas BA, Flowers CR, Keegan THM. Subsequent primary malignancies after diffuse large B-cell lymphoma in the modern treatment era. Br J Haematol 2017;178:72-80.
6. Major A, Smith DE, Ghosh D, Rabinovitch R, Kamdar M. Risk and subtypes of secondary primary malignancies in diffuse large B-cell lymphoma survivors change over time based on stage at diagnosis. Cancer 2020;126:189-201.
7. Wei G, Shu X, Zhou Y, Liu X, Chen X, Qiu M. Intra-Abdominal Desmoplastic Small Round Cell Tumor: Current Treatment Options and Perspectives. Front Oncol 2021;11:705760.
8. Zhang PJ, Goldblum JR, Pawel BR, Fisher C, Pasha TL, Barr FG. Immunophenotype of desmoplastic small round cell tumors as detected in cases with EWS-WT1 gene fusion product. Mod Pathol 2003;16:229-35.
9. Rodriguez E, Sreekantaiah C, Gerald W, Reuter VE, Motzer RJ, Chaganti RS. A recurring translocation, t(11;22)(p13;q11.2), characterizes intra-abdominal desmoplastic small round-cell tumors. Cancer Genet Cytogenet 1993;69:17-21.
10. Tateishi U, Hasegawa T, Kusumoto M, Oyama T, Ishikawa H, Moriyama N. Desmoplastic small round cell tumor: imaging findings associated with clinicopathologic features. J Comput Assist Tomogr 2002;26:579-83.
11. Pickhardt PJ, Fisher AJ, Balfe DM, Dehner LP, Huettner PC. Desmoplastic small round cell tumor of the abdomen: radiologic-histopathologic correlation. Radiology 1999;210:633-8.
12. Donnelly SC. 18F-FDG-PET/CT scanning-clinical usefulness beyond cancer. QJM 2018;111:593.
13. Ben-Sellem D, Liu KL, Cimarelli S, Constantinesco A, Imperiale A. Desmoplastic small round cell tumor: impact of F-FDG PET induced treatment strategy in a patient with long-term outcome. Rare Tumors 2009;1:e19.
14. Ostermeier A, McCarville MB, Navid F, Snyder SE, Shulkin BL. FDG PET/CT imaging of desmoplastic small round cell tumor: findings at staging, during treatment and at follow-up. Pediatr Radiol 2015;45:1308-15.
15. Liu Y, Tao Y, Wang F, Huang Z. Desmoplastic Small Round Cell Tumor of the Kidney With Mainly Pulmonary Symptoms by (18)F-FDG PET/CT. Urology 2021;154:e15-6.
16. Zhang WD, Li CX, Liu QY, Hu YY, Cao Y, Huang JH. CT, MRI, and FDG-PET/CT imaging findings of abdominopelvic desmoplastic small round cell tumors: correlation with histopathologic findings. Eur J Radiol 2011;80:269-73.
17. Kis B, O'Regan KN, Agoston A, Javery O, Jagannathan J, Ramaiya NH. Imaging of desmoplastic small round cell tumour in adults. Br J Radiol 2012;85:187-92.
18. Xuesong D, Hong G, Weiguo Z. Primary desmoplastic small round cell tumor of the tibia: PET/CT and MRI presentation of a rare case and review of the literature. J Bone Oncol 2020;20:100272.
19. Kushner BH, Laquaglia MP, Gerald WL, Kramer K, Modak S, Cheung NK. Solitary relapse of desmoplastic small round cell tumor detected by positron emission tomography/computed tomography. J Clin Oncol 2008;26:4995-6.
20. Reisner D, Brahee D, Patel S, Hartman M. A Case of Desmoplastic Small Round Cell Tumor. J Radiol Case Rep 2015;9:1-7.
21. Hatanaka KC, Takakuwa E, Hatanaka Y, Suzuki A, IIzuka S, Tsushima N, Mitsuhashi T, Sugita S, Homma A,

Morinaga S, Hashegawa T, Matsuno Y. Desmoplastic small round cell tumor of the parotid gland-report of a rare case and a review of the literature. Diagn Pathol 2019;14:43.
22. de Araújo RA, Araújo BJ. Desmoplastic small round cell tumor: report of 2 cases treated with chemotherapy alone or in combination with bevacizumab. Case Rep Oncol 2014;7:102-8.
23. Chen W, Chen H, Zhao C, Xie S, Qin J, Liu W. Desmoplastic small round cell tumor: the report of two cases and literature analysis review of the radiological findings. Quant Imaging Med Surg 2023;13:4762-9.
24. Harindran VD, Moideenkutty SV, Thanseer NTK, Prashanth P, Warrier N. Desmoplastic Small Round Cell Tumors-Case series of a Rare Tumor and Review of Literature. Asian Pacific Journal of Cancer Care 2023;8:627-31.
25. Mathys J, Vajtai I, Vögelin E, Zimmermann DR, Ozdoba C, Hewer E. Desmoplastic small round cell tumor: a rare cause of a progressive brachial plexopathy. Muscle Nerve 2014;49:922-7.
26. Fan HS, I'Ons B, McConnell R, Kumar V, Alzahrani S, Morris DL. Peritonectomy and hyperthermic intraperitoneal chemotherapy as treatment for desmoplastic small round cell tumour. Int J Surg Case Rep 2015;7C:85-8.
27. Brunetti AE, Delcuratolo S, Lorusso V, Palermo L, Di Giorgio A, Pisconti S, Silvestris N. Third-line trabectedin for a metastatic desmoplastic small round cell tumour treated with multimodal therapy. Anticancer Res 2014;34:3683-8.
28. Asadbeigi SN, Zhang L, Linos K. Subcutaneous desmoplastic small round-cell tumor: An unusual primary location expanding the differential of superficial round-cell tumors. J Cutan Pathol 2020;47:768-75.
29. Makis W, Girgis S. Intra-abdominal desmoplastic small round cell tumour: staging and surveillance with (18) F-FDG PET/CT following peritonectomy and HIPEC. BJR Case Rep 2016;2:20150434.
30. Küpeli S, Cağlar K, Birgen D, Sungur A, Varan A. Desmoplastic small round cell tumor of the mandible in a child with unusual plantar metastasis. J Pediatr Hematol Oncol 2010;32:e155-7.
31. Ramspott JP, Jäger T, Neureiter D, Emmanuel K, Schredl P. Presentation of a rare, highly aggressive peritoneal disease: desmoplastic small round cell tumor and its therapeutic options. Eur Surg 2021;53:251-5.
32. Hassan J, Kieft A, Joiner M, Miller S. Palliative Radiation Therapy in the Treatment of Desmoplastic Small Round Cell Tumors. Cureus 2023;15:e43863.
33. Cracco A, Roy M, Simpfendorfer CH. Cytoreductive surgery and hyperthermic intraperitoneal chemotherapy combined with two-stage hepatectomy for multiple and bilobar desmoplastic small round cell tumor liver metastases. J Gastrointest Oncol 2017;8:E60-4.
34. Zhou J, Li Q, Luo B, Fu X, Ou C, Gao X, Xu Z, Feng D, Yang K. Primary desmoplastic small round cell tumor of the submandibular gland: a case report and literature review. Diagn Pathol 2022;17:6.
35. Vujić G, Mikuš M, Matak L, Bonevski A, Babić I, Planinić P, Babić D, Ćorušić A. Desmoplastic Small Round Cell Tumor of the Ovary: A Case Report with a New Modality of Treatment and Review of the Literature. Rev Bras Ginecol Obstet 2020;42:297-302.
36. Subbiah V, Brown RE, Jiang Y, Buryanek J, Hayes-Jordan A, Kurzrock R, Anderson PM. Morphoproteomic profiling of the mammalian target of rapamycin (mTOR) signaling pathway in desmoplastic small round cell tumor (EWS/WT1), Ewing's sarcoma (EWS/FLI1) and Wilms' tumor(WT1). PLoS One 2013;8:e68985.
37. Umeda K, Saida S, Yamaguchi H, Okamoto S, Okamoto T, Kato I, Hiramatsu H, Imai T, Kodaira T, Heike T, Adachi S, Watanabe KI. Central nervous system recurrence of desmoplastic small round cell tumor following aggressive multimodal therapy: A case report. Oncol Lett 2016;11:856-60.
38. Miwa S, Kitamura S, Shirai T, Hayashi K, Nishida H, Takeuchi A, Nojima T, Tsuchiya H. Desmoplastic small round cell tumour successfully treated with caffeine-assisted chemotherapy: a case report and review of the literature. Anticancer Res 2010;30:3769-74.
39. Bengu Cobanoglu H, Hanna EY, Bell D, Esmaeli B. Desmoplastic Small Round Cell Tumor Presenting as an Ocular Mass: Unusual Localization and Remarkable Surgical Approach. Curr Oncol Rep 2017;19:80.
40. Piciu D, Barbus E, Pestean C, Piciu A. F18-FDG PET/CT in retroperitoneal desmoplastic small round blue cell tumour occurring in a patient with in situ breast carcinoma. BMJ Case Rep 2015.
41. Laurens JR, Frankel AJ, Smithers BM. Intra-abdominal desmoplastic small round cell tumour in a 56-year-old female: Case report of a very rare presentation of an unusual tumour. Int J Surg Case Rep 2021;79:323-6.
42. Gan HL, Ru GQ, Wang J, Zhao M. Desmoplastic small round cell tumour presenting as cervical lymph nodes metastases with solid pattern morphology and novel EWSR1-WT1 fusion transcript. Pathology

2022;54:482-5.
43. Çolak Ö, Şahin AE, Mutlu ÖÖ, Sayılgan T. A Rare Tumor, a Rare Localization: A Malignant Small Round Cell Tumor in the Thigh. Eur Arch Med Res 2018;34:200-2.
44. Hou W, Dai J, Tian R. Metastatic Pulmonary Desmoplastic Small Round Cell Tumor on FDG PET/CT. Clin Nucl Med 2023;48:828-9.
45. Sharma AE, deVries JA, Agrawal C, Haydon RC, Krausz T, Pytel P, Cipriani NA. Primary Desmoplastic Small Round Cell Tumor of the Femur: Case Report and Review of a Rare Intraosseous Malignancy. Int J Surg Pathol 2022;30:317-25.
46. Zheng Z, Hu P, He Y, Shi H. Desmoplastic small round cell tumor with ovarian involvement on [18F]-FDG PET/CT. Rev Esp Med Nucl Imagen Mol (Engl Ed) 2024;43:55-6.
47. Subbiah V, Murthy R, Anderson PM. [90Y]yttrium microspheres radioembolotherapy in desmoplastic small round cell tumor hepatic metastases. J Clin Oncol 2011;29:e292-4.
48. Ferrari A, Bergamaschi L, Chiaravalli S, Pecori E, Diletto B, Alessandro O, Giandini T, Livellara V, Sironi G, Casanova M. Multiagent chemotherapy including IrIVA regimen and maintenance therapy in the treatment of desmoplastic small round cell tumor. Tumori 2022;108:93-7.
49. Slotkin EK, Mauguen A, Ortiz MV, Cruz FSD, O'Donohue T, Kinnaman MD, Meyers PA, Wexler LH, Rodriguez S, Avutu V, Kelly CM, D'Angelo SP, Keohan ML, Gounder MM, Nacev BA, Rosenbaum E, Dickson MA, Thornton KA, Bender JLG, Tap WD. A phase I/II study of prexasertib in combination with irinotecan in patients with relapsed/refractory desmoplastic small round cell tumor and rhabdomyosarcoma. J Clin Oncol 2022;40:abstr 11503.
50. Adamson PC, Blaney SM, Widemann BC, Kitchen B, Murphy RF, Hannah AL, Cropp GF, Patel M, Gillespie AF, Whitcomb PG, Balis FM. Pediatric phase I trial and pharmacokinetic study of the platelet-derived growth factor (PDGF) receptor pathway inhibitor SU101. Cancer Chemother Pharmacol 2004;53:482-8.
51. Fine RL, Shah SS, Moulton TA, Yu IR, Fogelman DR, Richardson M, Burris HA, Samuels BL, Assanasen C, Gorroochurn P, Hibshoosh H, Orjuela M, Garvin J, Goldman FD, Dubovsky D, Walterhouse D, Halligan G. Androgen and c-Kit receptors in desmoplastic small round cell tumors resistant to chemotherapy: novel targets for therapy. Cancer Chemother Pharmacol 2007;59:429-37.

Cite this article as: Huang W, Zhang Y, Qiu Y, Liu Y, Sun Z, Song L, Wang A, Zhang J, Kang L. Multimodality imaging of ureteral desmoplastic small round cell tumor: a case description and literature analysis of ^{18}F-fluoro-2-deoxy-d-glucose positron emission tomography-computed tomography findings. Quant Imaging Med Surg 2024;14(4):3180-3193. doi: 10.21037/qims-23-1649

